Bespoke doxorubicin-loaded gold nanoparticles for ultrasound-guided cancer cell killing

Biomedicine & Pharmacotherapy 193 (2025) 118777

Contents lists available at ScienceDirect

Biomedicine & Pharmacotherapy

journal homepage: www.elsevier.com/locate/biopha

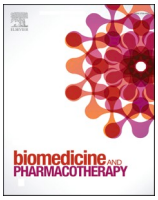

Bespoke doxorubicin-loaded gold nanoparticles for ultrasound-guided cancer cell killing

Federica Foglietta [a], Agnese Fragassi [b], Cristiano Pesce [b], Francisco Andres Soto Arratia [a], Alberto Mangia [c], Maurizio Giustetto [d], Gianni Durando [e], Gian Matteo Morano [f], Paolo Caliceti [b], Andrea Grandoni [g], Roberto Canaparo [a,*], Loredana Serpe [a,1], Stefano Salmaso [b,1]

[a] Department of Drug Science and Technology, University of Torino, Torino, Italy
[b] Department of Pharmaceutical and Pharmacological Sciences, University of Padova, Padova, Italy
[c] Department of Molecular Biotechnology and Health Sciences, Molecular Biotechnology Center, University of Turin, Turin 10126, Italy
[d] Department of Neuroscience, University of Turin, Turin 10126, Italy
[e] National Institute of Metrological Research (INRIM), Torino, Italy
[f] Esaote SpA, Genova, Italy
[g] Esaote SpA, Firenze, Italy

ARTICLE INFO

Keywords:
Gold nanoparticles
Folate targeting
Doxorubicin
Ultrasound
Sonodynamic therapy
Cancer

ABSTRACT

Both doxorubicin and gold nanoparticles (GNPs) exhibit sonosensitising properties, significantly increasing the production of cytotoxic reactive oxygen species (ROS) when exposed to ultrasound (US). Ultrasound-responsive, targeted GNPs decorated with a pH-releasable doxorubicin prodrug (FDGNPs) have been developed to exploit this synergistic effect, enabling highly selective and effective anticancer activity. The GNPs were produced using the Turkevich method and functionalised with folate-PEG$_{3.5\,kDa}$-SH as the targeting agent (FGNPs). These were then decorated with doxorubicin derivatised with lipoic acid via a pH-sensitive linker and stabilised with a mPEG$_{2\,kDa}$-SH coating. The FDGNPs' cell targeting, uptake and anticancer effects were evaluated in an epidermoid carcinoma cell line expressing a high level of folate receptor (KB-hFR), which was cultured as monolayers and three-dimensional spheroids. The anticancer effects of the US-exposed FDGNPs were evaluated in terms of cell viability, ROS production and cell death. FDGNPs selectively associated to KB cells in a folate-dependent manner. Ultrasound-exposed FDGNPs resulted in a significant decrease in KB-hFR cell viability of up to 70 %, increased ROS of up to 50 %, and increased necrotic cells of up to 45 %, compared to untreated cells. Furthermore, switching from a custom-built US device to a standardised US scanning device confirmed that US exposure effectively elicits the anticancer activity of FDGNPs in KB-hFR spheroids, resulting in a 45 % decrease in cell viability. GNPs have been engineered to provide active targeting and controlled drug release while exploiting their sonosensitising properties; therefore, this platform shows promise in improving the selectivity and efficacy of cancer therapy.

1. Introduction

Delivering therapeutic concentrations of drugs to tumour tissue without causing systemic toxicity is a key issue in cancer therapy. Doxorubicin, for instance, is a photosensitive anthracycline used in clinical protocols to treat a variety of cancers, including carcinomas, sarcomas and hematological cancers. Doxorubicin's non-selective cytotoxicity is primarily exerted by inhibiting topoisomerase II activity and

* Correspondence to: Department of Drug Science and Technology, University of Torino, Via Pietro Giuria 13, Torino 10125, Italy.
E-mail addresses: federica.foglietta@unito.it (F. Foglietta), agnese.fragassi@unipd.it (A. Fragassi), cristiano.pesce@unipd.it (C. Pesce), franciscoandres.sotoarratia@unito.it (F.A.S. Arratia), alberto.mangia@unito.it (A. Mangia), maurizio.giustetto@unito.it (M. Giustetto), g.durando@inrim.it (G. Durando), gianmatteo.morano@esaote.com (G.M. Morano), paolo.caliceti@unipd.it (P. Caliceti), andrea.grandoni@esaote.com (A. Grandoni), roberto.canaparo@unito.it (R. Canaparo), loredana.serpe@unito.it (L. Serpe), stefano.salmaso@unipd.it (S. Salmaso).
[1] Loredana Serpe and Stefano Salmaso equally contributed to this study

https://doi.org/10.1016/j.biopha.2025.118777
Received 26 August 2025; Received in revised form 27 October 2025; Accepted 7 November 2025
Available online 12 November 2025

by inducing the generation of free radicals. Consequently, doxorubicin exhibits several adverse effects, including haematological toxicity and progressive cardiac damage [1].

Nanotechnology provides innovative solutions to this challenge in the form of a wide variety of drug delivery systems (DDSs). These include liposomes, polymeric nanoparticles, micelles, dendrimers, inorganic nanoparticles, quantum dots and gold or metal oxide structures [2], which exploit the enhanced permeability and retention (EPR) effect to control the pharmacokinetics and biodistribution of the loaded drug. Promising results have been achieved in preclinical in vivo models, with some of these DDSs progressing to the clinical stage [3].

The surface functionalisation of drug nanocarriers is a widely used technique to improve the biopharmaceutical properties of these systems, including in vitro and in vivo colloidal stability and cell targeting. Polyethylene glycol (PEG) has been used to increase the colloidal stability of nanoparticles and prevent in vivo opsonisation, resulting in prolonged systemic circulation [4]. Surface functionalisation with targeting agents in the form of small molecules or macromolecules, such as proteins, antibody derivatives and polysaccharides, selectively binds to receptors on the surface of cancer cells, increasing drug delivery to cancer cells while reducing off-target toxicity [5]. The folate receptor (FR) is overexpressed on the surface of several types of cancer cells, thus representing a suitable target for the selective delivery of anticancer drugs [6]. The efficacy of FR targeting is supported by the recent FDA approval of the antibody-drug conjugate mirvetuximab soravtansine-gynx (MIRV) for the treatment of fallopian tube cancer, ovarian cancer and peritoneal cancer [7]. Folic acid is a small molecule with high biocompatibility and non-immunogenic properties that can easily be activated for conjugation to nanocarriers using well-defined chemistry [8].

Folate-functionalised nanocarriers (e.g., liposomes, micelles, polymeric, inorganic and lipid nanoparticles) have been investigated for doxorubicin drug delivery [5]. However, despite doxorubicin delivered through folate-functionalised nanocarriers showing enhanced cellular uptake and cytotoxicity compared to the free drug in tumour cells, formulations with a suitable clinical outcome have not yet been obtained. One of the major limitations with these products is the lack of precise control over doxorubicin release. Stimuli-sensitive systems that exploit biocompatible components capable of undergoing chemical or conformational changes in response to a local stimulus (i.e., the tumour microenvironment) or external physical activation may overcome this hurdle [9].

Gold nanoparticles (GNPs) have a variety of applications in fields such as material science, bioanalytical chemistry, industrial catalysis and medicine. This is due to their high electron density, dielectric and catalytic properties, and their ability to bind various biomolecules without affecting their biological activity [10]. GNPs that are chemically or physically coated with anticancer drugs, including doxorubicin, can be used in cancer treatment [11–15]. For example, Wang et al. [14] conjugated doxorubicin to 30 nm non-targeted GNPs via a pH-sensitive linker, yielding controlled drug release at the acidic pH typical of the tumour microenvironment and tumour cell availability [16,17]. However, inaccurate pH-controlled release may result in off-target drug release with potential systemic toxicity, or conversely, incomplete release of payloads in the tumour cells [18]. Although off-target drug release may be mitigated by passive and active delivery, incomplete drug release results in a poor clinical outcome [18,19].

Exploiting external physical triggering can enable precise control of on-demand drug release. Sonodynamic therapy (SDT) consists of exposing a stimulus-sensitive compound to ultrasound (US), which can induce oxidative damage leading to cancer cell death [20,21]. For example, GNPs stimulated with US have been found to induce reactive oxygen species (ROS)-mediated cancer cell death [19,22]. Compared to other external triggers such as light, which is used for on-demand drug delivery in photodynamic or photothermal therapy with doxorubicin loaded GNPs [22,23], US is a more practical and cost-effective externally applicable stimulus penetrating deeper into tissue than other strategies, such as using long-wavelength light or two-photon strategies (e.g., a near-infrared laser).

Our aim in this scenario is to develop US-responsive, folate-targeted GNPs loaded with doxorubicin via a pH-responsive linker. This will create a nanosystem that can be activated on-demand and kill FR-overexpressing cancer cells. Doxorubicin is conjugated to the GNPs to enable drug release at the acidic pH of cancer cells, thereby exploiting selective US activation to significantly increase ROS-mediated cytotoxicity.

2. Materials and methods

2.1. Materials

Folic acid (FA), sodium citrate tribasic dihydrate, tetrachloroauric (III) acid trihydrate, iodine, potassium iodide, barium chloride, N-hydroxysuccinimide (NHS), N, N'-dicyclohexylcarbodiimide (DCC), triethylamine, α-lipoic acid, dimethylsulfoxide anhydrous (DMSO), chloroform, dichloromethane (DCM), diethyl ether (Et_2O), Sephadex G-25 superfine and Sephadex LH 20 gel filtration resins were purchased Merck (Darmstadt, Germany). Doxorubicin hydrochloride was purchased from LC Laboratories (Woburn, MA, USA). BDP 630/650 X NHS ester was obtained from Lumiprobe (Hannover, Germany). NH_2-$PEG_{2\,kDa}$-SH and NH_2-$PEG_{3.5\,kDa}$-SH were purchased from JenKem-Technology (Plano, TX, USA) and $mPEG_{2\,kDa}$-SH was acquired from Iris Biotech GmbH (Marktredwitz, Germany). All the chemical reagents for cell culture, Dulbecco's modified Eagle's medium (DMEM) and folic acid-free DMEM, L-glutamine solution, D-(+)-glucose solution, sodium bicarbonate solution, foetal bovine serum (FBS), penicillin-streptomycin solution and trypsin-EDTA solution were supplied by Merck (Darmstadt, Germany).

2.2. Synthesis and physicochemical characterization of folate receptor-targeted doxorubicin-loaded gold nanoparticles

Synthesis and characterization of functional components. The synthesis and characterization of the targeting agent FA-$PEG_{3.5\,kDa}$-SH (FA-PEG-SH) and the fluorescent probe BDP-$PEG_{2\,kDa}$-SH (BDP-PEG-SH) were performed according to the literature [24,25].

N-hydroxy succinimidyl ester activated folate was reacted with NH_2-$PEG_{3.5\,kDa}$-SH in DMSO in the presence of triethylamine to yield the conjugate FA-$PEG_{3.5\,kDa}$-SH which was purified by size exclusion chromatography using Sephadex G-25 superfine resin eluted with water. The FA-PEG-SH was characterized by UV-Vis spectroscopy at 363 nm to assess folate and by iodine assay to quantify the PEG [26]. The chemical identity of the product was confirmed by MALDI mass spectroscopy (m/z $[M\text{-}H^+] = 4117$) and by ^1H NMR.

BDP 630/650 X NHS was reacted with NH_2-$PEG_{2\,kDa}$-SH in anhydrous DMSO added of triethylamine yielding BDP-$PEG_{2\,kDa}$-SH which was purified by size exclusion chromatography using LH20 resin run with ethanol. BDP-$PEG_{2\,kDa}$-SH (BDP-PEG-SH) was characterized by UV-Vis spectroscopy at 628 nm to assess BDP concentration, and by iodine assay to determine PEG concentration. The chemical identity of the product was confirmed by MALDI spectrometry (m/z $[M\text{-}H^+] = 2448$) and by ^1H NMR spectroscopy.

Doxorubicin (Doxo) was converted into an acid pH releasable disulfide terminated prodrug (lipoyl-hydrazone-Doxo) by multistep procedure. α-Lipoic acid (10.0 mmol) was dispersed in 50 mL methanol, the mixture was added of thionyl chloride (15.0 mmol) and refluxed for 18 h. Methanol was removed by rotary evaporation and residue redissolved in ethyl acetate was washed with saturated $NaHCO_3$; the solvent was removed under vacuum resulting in quantitative conversion yield. Lipoyl methyl ester (10.0 mmol) was dissolved in hydrazine monohydrate (100.0 mmol) and refluxed. After quenching with saturated NH_4Cl, the mixture was extracted with $CHCl_3$ and solvent removed

under vacuum. The crude product was purified by flash chromatography (90:10 v/v $CHCl_3$/MeOH + 0.1 % aq. NH_3) and fractions identified by TLC run; yield was 98 %. Lipoyl-hydrazide was conjugated to the ketone of Doxo (0.1 M) in methanol using a 2.5:1 lipoyl-hydrazide/ Doxo molar ratio in the presence of TFA as catalyst. The crude product was purified under reflux in methanol/diethyl ether.

The conjugates were analysed by ^{1}H-NMR, mass and UV/vis spectrometry to assess chemical identity and purity.

Solutions of lipoyl-hydrazone-Doxo in 10 mM ammonium acetate at pH 5 or in 10 mM ammonium bicarbonate at pH 7.4 were incubated at 37 °C and analysed by mass spectrometry (Micromass Q-TOF micro™ ESI-TOF; Waters, Milford, MA-USA) to quantify Doxo released by lipoyl-hydrazone-Doxo over time under the two pH conditions.

Synthesis, decoration, characterization of GNPs. GNPs were prepared by reducing $HAuCl_4$ with trisodium citrate following a slightly modified Turkevich protocol [27,28]. The concentration of the GNPs in the colloidal dispersions was quantified according to combined DLS and UV-Vis spectroscopy data as reported in the literature and our previous studies [25,29]. The particle surface was functionalized with the thiol/disulfide-terminating components using the procedure described in our previous works [24,30] to obtain the folate receptor-targeted Doxo-loaded PEG stabilized gold nanoparticles (FDGNPs). Briefly, a volume of 10 nM GNPs in milliQ water was sequentially added of each thiol bearing reagent dissolved in mQ water to achieve the following molar ratios: 1) 50:5:1 FA-$PEG_{3.5\,kDa}$-SH:$mPEG_{2kDa}$-SH_GNP; 2) 20:80:1 BDP-PEG-SH:$mPEG_{2kDa}$-SH:GNP (where applicable); 3) 1000:1 lipoyl-hydrazone-Doxo:GNP; 4) 1000:1 $mPEG_{2kDa}$-SH:GNP. After the addition of each reagent, mixture was kept under mild agitation for 3 h. Folate free control nanoparticles (DGNPs) were generated adding $mPEG_{3.5\,kDa}$-SH in place of FA-$PEG_{3.5\,kDa}$-SH and drug-free folate-receptor targeted nanoparticles (FGNPs) were obtained by omitting the proDoxo [24].

After each conjugation step, particles were centrifuged at 13,500 rcf for 30 min at 4 °C, and unbound ligands in the supernatant were quantified by spectroscopic (FA-$PEG_{3.5\,kDa}$-SH at 363 nm, $mPEG_{2kDa}$-SH via iodine assay) and spectrofluorimetric (BDP-PEG-SH, λ_{ex} 628 nm/ λ_{em} 642 nm; lipoyl-hydrazone-Doxo, λ_{ex} 488 nm/ λ_{em} 590 nm) analyses.

Lyophilized particles were obtained by mixing equal volumes of functionalised particles with 1 % w/v mixture of PVP 40 kDa (Merck, Darmstadt, Germany)/ Tween 20 (Croda International PLC, Snaith, UK) (1:1) in Milli-Q water (0.5 % w/v final). The mixtures were frozen in liquid nitrogen for 2 min and lyophilized overnight (Hetossic lyophilizer, HETO Lab Equipment, Birkerod, Denmark). The dried particle reconstitution was carried out by redispersion in Ca^{2+}/Mg^{2+}-free DPBS. The dispersion was centrifuged twice (13,500 rcf, 30 min, 4 °C) with supernatant replacement to remove residual cryoprotectants [24].

Hydrodynamic diameters and zeta potential were assessed by dynamic light scattering (DLS) (Zetasizer Nano ZS; Malvern Instruments Co., Malvern, Worcestershire, UK). The results were expressed in Intensity distribution for the functionalized particles. UV–vis spectra were acquired on a Thermo Scientific™ Evolution™ 201 UV–visible spectrophotometer (Thermofisher, Rockford, IL, USA) or a Nanodrop 2000c spectrophotometer (Thermofisher, Rockford, IL, USA). Analyses were performed with 6-fold dilutions of samples in mQ water. GNPs imaging was performed by applying particles to EM grids, negatively stained, and imaged by transmission electron microscopy (TEM; Tecnai G2 microscope FEI - FEI Tecnai, OR-USA). The stability of 2 μM FDGNP, DGNP and FGNP in folic acid free DMEM supplemented of 10 % FBS and incubated at 37 °C was assessed over time by DLS.

2.3. Cell culture

The epidermoid carcinoma (KB) cells were purchased from the European Collection of Cell Cultures, (ECACC, Salisbury, UK) and the human breast adenocarcinoma (MCF7) cells from the Interlab Cell Line Collection (ICLC, Genova, Italy). The KB cells were cultured as a monolayer in DMEM medium (Merck, Darmstadt, Germany), supplemented with 10 % FBS, 2 mM L-glutamine, and 1 % antibiotics (Merck, Darmstadt, Germany). To induce a high level of FR expression (KB-hFR cells), the KB cells were cultured in a specific medium containing sterile water, 10 % DMEM low glucose medium without L-glutamine, sodium bicarbonate, and folic acid (Merck, Darmstadt, Germany), 15 % FBS, 2 mM L-glutamine, 1 % antibiotics, 0.2 % D-glucose and 5 % sodium bicarbonate (Merck, Darmstadt, Germany) for 10 days. The MCF7 cells were grown in RPMI-1640 medium (Merck, Darmstadt, Germany) supplemented with 10 % FBS, 2 mM L-glutamine, and 1 % antibiotics.

All the cell lines were maintained at 37 °C with 5 % CO_2 in a dark, humid atmosphere (Thermo Fisher Scientific, USA). The cultures were passaged at regular intervals using a 0.05 % trypsin-0.02 % EDTA solution (Merck, Darmstadt, Germany).

2.4. Cell proliferation assay

KB-hFR cells were incubated with increasing concentrations of free Doxo or FDGNP in order to assess their cytotoxicity. Briefly, 1.2×10^2 KB-hFR cells were seeded in 96-well culture plates in 100 μL of culture medium in replicates (n = 8) and incubated with Doxo or FDGNPs (0.001, 0.01, 0.1, 1, 10 μM) after two days. Cell proliferation was assessed using the WST-1 assay (Roche Applied Science, Basel, Switzerland) by adding the WST-1 reagent (10 μL) at two time points (24 and 72 h after treatment), followed by an incubation period of 3 h at 37 °C. The absorbance (abs) of each well was measured at 450 nm with a microplate reader (NeoBiotech, Nanterre, France), using 620 nm as the reference wavelength. The cytotoxicity of free Doxo or FR-targeted Doxo-loaded gold nanoparticles (FDGNPs) was displayed as a percentage according to the following equation: % cytotoxicity = 100 × (abs control - abs sample). The WST-1 assay was also performed to evaluate the effect of the US-based treatments on cell proliferation (24, 48 and 72 h after treatment).

2.5. US treatment and characterisation of the US field

For the US experiments, the US field was generated by two different US devices, depending on the cell culture type: monolayer-derived cell suspensions as two-dimensional (2D) cultures and spheroids as three-dimensional (3D) cultures.

To treat the 2D cell cultures, the US field was generated by a plane wave transducer (INRIM, Torino, Italy), connected to a broadband power amplifier (type 350 L; Electronics & Innovation Ltd., Rochester, USA) and a function generator (type 33250, Agilent Technologies, USA). It worked in pulse mode at a frequency of 1.5 MHz with a spatial peak temporal average intensity (ISPTA) of 0.11 W/cm^2 and a duty cycle of 50 %, for 3 min. Sample tubes containing 5×10^5 KB-hFR cells in 2.7 mL of PBS were placed in a custom-built mechanical adaptor 2 cm from the transducer surface. The adaptor was filled with cold deionized water, which was replaced for each treatment to avoid possible temperature increase due to US exposure.

In order to treat the 3D cell cultures, the MyLab OMEGA US scanner equipped with a phase array mod. P1–5 (Esaote, Firenze, Italy) was selected, as its features best replicate those of the previous custom-built device. It should be noted that using this type of US device results in a ISPTA and a medical index (MI) that comply with regulatory specifications. This ensure that dangerous US bioeffects are strictly avoided, and the contribution of thermal mechanisms to biological effects is eliminated. The transducer operated in pulse mode at a frequency of 1.7 MHz with a ISPTA of 0.26 W/cm^2 and a duty cycle of 50 %, for 5 min. The spheroids were treated in a 96-well culture plate filled with PBS. The plate was hermetically sealed in a custom-built mechanical adaptor (Prensilia, Pisa, Italy) and positioned 4 cm from the transducer surface. This adaptor is a tank lined with sound-absorbing material in which the culture plate can be positioned and anchored at a controlled location on the tank's base. The tank was filled with deionised water, which was

replaced for each treatment. The tank contains a mechanism that can hold the US probe and position the US beam with repeatable precision over the selected wells. This is made possible by a micrometric adjustment system that moves the transducer along the X, Y and Z axes. Furthermore, US scanner B-mode imaging can be used to precisely position the focal area relative to the cells, ensuring they are treated according to the selected parameters (e.g., peak positive pressure, ISPTA and MI). Following US treatment, the cells and spheroids are processed according to the desired analysis type.

Complete characterisation of the US field generated by the two US devices in their respective operating modes (i.e., peak positive pressure, ISPTA and MI) was obtained using an ONDA type AIMS III scanning tank system with an ONDA type HNA-0400 needle hydrophone and an ONDA type AH-2020 preamplifier (HI GAIN configuration).

2.6. Flow cytometry

Flow cytometry assays were carried out using a C6 flow cytometer (Accuri Cytometers, Milan, Italy). All samples were analysed by at a medium flow rate with 1×10^4 events considered, and all debris with low forward scatter (FSC) and low side scatter (SSC) was removed from the analysis.

2.6.1. Folate receptor expression on cancer cells

The presence of FRs was investigated by flow cytometry in MCF7, KB and KB-hFR cells. MCF7 cells were used as a negative control, as they exhibit low FR expression. In brief, 7.0×10^4 MCF7, KB and KB-hFR cells were cultured in 6-well culture plates in 2 mL of their respective medium for 3 days. The cells were then incubated for 2 h at 37 °C with 10 μg/mL folate receptor α monoclonal antibody (Enzo Life Sciences, NY, USA). After incubation, the cells were washed with PBS and then incubated with 0.5 μg/mL rabbit F(ab') 2 polyclonal secondary antibody conjugated with Alexa Fluor® 488 nm (Abcam, Cambridge, UK) for 1 h at 37°C. After the incubation period, the cells were detached using trypsin and the resulting pellet was resuspend and analysed by flow cytometry (λ_{ex} 499 nm, λ_{em} 520 nm). The results are expressed as integrated mean fluorescence intensity (iMFI), i.e. the product of the frequency of positive cells and the mean fluorescence intensity of the cells.

2.6.2. Doxorubicin uptake in cancer cells

The cellular uptake of Doxo as FDGNPs was evaluated by measuring the cellular fluorescence attributed to the Doxo associated cells using flow cytometry. MCF7, KB and KB-hFR cells were incubated with FDGNPs and analysed by flow cytometry (λ_{ex} 488 nm, $\lambda_{em} > 670$ nm) at different time points (2, 6 and 24 h). The results are expressed as an integrated mean fluorescence intensity (iMFI) ratio to provide information on ratiometric variations in fluorescence at each time point relative to the control cells (i.e., the untreated cells). In brief, 3×10^4 cells were seeded in 6-well culture plates in 2.0 mL of culture medium and allowed to grow for 2 days. The cells were then incubated with FDGNPs at an equivalent Doxo concentration of 2.0 μM. At the end of each incubation period, the cells were detached, and each pellet was resuspended in 200 μL of PBS for flow cytometry analysis.

2.6.3. Intracellular ROS generation

The CellROX® Green Assay (Life Technologies, Milano, Italy) was used to detect ROS production by flow cytometry. This assay measures the fluorescence of the CellROX® green reagent (λ_{ex} 545 nm, λ_{em} 565 nm). KB-hFR cells were incubated with drug-free FGNPs and 2.0 μM Doxo-loaded FGNPs (FDGNPs) for 24 h, after which the cells were exposed to US (1.5 MHz, 0.11 W/cm^2, 50 %, 3 min). Then, 5×10^5 cells for each treatment condition were resuspended in 2.7 mL of PBS and centrifuged at 1500 rpm for 5 min and the supernatant was discharged. Finally, 1 mL of CellROX® green intermediate solution (2 μL CellROX® green stock + 1000 μL KB-hFR medium without FBS) was added. Since the CellROX® solution is highly photosensitive, the samples were covered from light and incubated at 37 °C for 30 min. The tubes were then centrifuged, and the pellet was resuspended in 2.7 mL of PBS. The samples were then analysed by flow cytometry at the following time points: 1, 5, 15, 30, 60, 90 and 120 min from the start of the various treatments (untreated cells, cells exposed to FGNPs or FDGNPs only, cells exposed to US only and cells exposed to FGNPs and US or FDGNPs and US).

2.6.4. Cell death analysis

A cell death assay was performed 36 h after the various treatments using the Annexin-V-APC & SYTOX® Green Assay (Life Technologies, Milano, Italy). Briefly, after the various treatments (untreated cells, cells exposed to FGNPs or FDGNPs only, cells exposed to US only and cells exposed to FGNPs and US or FDGNPs and US), 1.2×10^5 cells per condition were seeded in 1 mL of culture medium. The cells were then incubated in 5 % CO_2 at 37 °C for 24 h, after which they were collected by trypsinisation, washed twice with PBS and the pellet was resuspended in 1 mL of PBS. Finally, 100 μL of the cell suspension were mixed with 5 μL of 1x annexin V binding buffer and 1 μL of 1 M SYTOX® green solution. The mixture was then incubated for 15 min at 37 °C and then mixed gently with 400 μL of 1x annexin binding buffer. Flow cytometry analysis was then performed to detect annexin-V-APC (λ_{ex} 650 nm, λ_{em} 660 nm) and SYTOX® green (λ_{ex} 503 nm, λ_{em} 554 nm).

2.7. Intracellular localisation of FDGNPs by fluorescence and confocal microscopy

Fluorescence and confocal microscopy analyses were performed to detect the intracellular access of FDGNPs and Doxo in KB-hFR cells. Briefly, the cells were incubated with FDGNPs at an equivalent Doxo concentration of 2.0 μM for 24 h. When required, 5×10^5 cells were suspended in 2.7 mL of PBS and underwent US exposure, as previously described. Following each treatment, 1.2×10^4 cells were seeded onto a glass slide in a well of a 24-well culture plate containing 1 mL of culture medium. Twenty-four hours after the treatment, each slide was incubated with 200 μL of a DAPI solution (1 μg/mL) at 37 °C for 15 min to stain the cell nuclei. The DAPI solution was then removed by washing with PBS and each slide was fixed with 200 μL of 4 % paraformaldehyde (PAF) for 15 min. The PAF was then removed, and the slides were washed with PBS before being mounted on coverslips using 5 μL of Fluoroshield® (Merck, Darmstadt, Germany). Fluorescence microscopy images were acquired using a Leica DM4000I (Leica, Milano Italy) at 63x magnification and confocal microscopy images using a LSM 900 (Zeiss, Milano, Italy) at 40x magnification. All the images were then processed using ImageJ software (version 1.54, Fiji, Bristol, UK) and analysed in the middle section.

2.8. Evaluation of spheroid growth

KB-hFR spheroids were generated by seeding 10000 cells per well into 96-U well plates that had been coated with 1.5 % agarose. The growth of the spheroids was monitored over time. Four days after seeding, selected spheroids were incubated with drug-free FGNPs and 4.0 μM Doxo-loaded FGNPs (FDGNPs) for 24 h, during which time they were kept in a dark incubator. After incubation, the spheroids were washed 3 times with PBS, after which 300 μL of PBS were added to each well prior to US exposure. The following experimental conditions were considered: i) untreated spheroids (Ctrl), ii) spheroids pre-incubated with FGNPs or FDGNPs for 24 h, iii) spheroids treated with US only and iv) spheroids pre-incubated with FGNPs or FDGNPs and then treated with US. A different US device was used to treat the spheroids directly in the plate with respect to the device used for 2D cell culture experiments. This approach eliminated the need to collect the spheroids in tubes, helping to maintain their structural stability on the agarose coating. The US field was generated at a frequency of 1.7 MHz, 0.26 W/cm^2, 50 %, for 5 min.

Forty-eight hours after the treatment, the CellTiter-Glo 3D Luminescent Cell Viability Assay (Promega, United States) was used to evaluate the spheroid cell viability. This assay quantifies intracellular ATP, which is an indirect indicator of cellular metabolism and, consequently, of the presence of viable cells. The spheroids were collected and transferred into a special optics 96-well plate before the assay was performed according to the manufacturer's instructions. Luminescence was measured using a Glomax luminometer (Promega, Milano, Italy). Data are presented as the average of luminescence signal in relative light units (RLU).

2.9. Statistical analysis

Data are shown as the mean value ± standard deviation from three separate experiments. Statistical analyses were performed using GraphPad Prism 5.0 software (San Diego, California, USA). According to the experimental design, multiple *t*-tests, one-way ANOVA and two-way ANOVA, followed by Bonferroni's post-hoc test, were used to calculate the significance threshold. The statistical significance threshold was set at $p \leq 0.05$.

3. Results

The novel targeted multifunctional gold nanoparticulate system FDGNP was designed to combine the tumor-selective doxorubicin delivery with ultrasounds treatment. FDGNPs were obtained by the integration of five distinct materials: i) gold nanoparticles (GNPs), as colloidal scaffold for multivalent surface modification and sonosensitizer; ii) folate-PEG$_{3.5\,kDa}$-SH (F), acting as a targeting ligand; iii) Bodipy X-PEG$_{2\,kDa}$-SH, incorporated as a fluorescent probe for traceability; iv) a pH-sensitive doxorubicin prodrug, lipoyl-hydrazone-doxorubicin (D), enabling stimuli-responsive drug release; (v) mPEG$_{2\,kDa}$-SH, providing colloidal stabilization and stealth properties. The lipoyl and thyol functions ensure stable conjugation of the drug and the polymer derivatives to gold nanoparticles. Control doxorubicin decorated non-targeted particles and doxorubicin-free targeted nanoparticles were also generated by omitting the folate-PEG$_{3.5\,kDa}$-SH (DGNPs) or doxorubicin (FGNPs), respectively.

3.1. Folate receptor-targeted doxorubicin-loaded gold nanoparticles

Synthesis of functional components for GNP decoration. The folate-containing targeting moiety, folate-PEG$_{3.5\,kDa}$-SH, was synthesized following a protocol previously established by our group [25,30]. The PEG backbone, with a molecular weight of 3.5 kDa, was selected to ensure adequate extension of the folate moiety from the nanoparticle surface, thereby facilitating recognition by folate receptors. Chemical identity was confirmed by mass spectrometry, which exhibited *m/z* centered at 4117 *m/z* while RP-HPLC purity exceeding 98 %.

A Bodipy (BDP)-tagged derivative as fluorescent label was generated through conjugation of BDP to the amino terminus of a thiol-terminated 2 kDa PEG chain. The shorter PEG spacer, relative to that applied for folate conjugation, was intended to minimize steric interference with folate–receptor interactions. The ^{1}H NMR analysis showed integral ratio of diagnostic signals indicating a conjugation efficiency above 90 %. The mass spectrum displayed a signal centered at 2448 *m/z*, while RP-HPLC analysis confirmed a purity > 99 %.

The pH-labile doxorubicin prodrug, lipoyl-hydrazone-Doxo (Scheme 1), was obtained through conjugation of Doxo to the heterobifunctional linker lipoyl hydrazide in order to yield a pH cleavable hydrazone bond for drug release under acid intracellular environment. The synthetic procedure resulted in lipoyl-hydrazone-Doxo derivative in a yield of 82 % and a final purity > 98 %, as determined by NMR. ESI-TOF mass spectrometry displayed a signal at *m/z* 746.24, consistent with the theoretical [M–H$^+$] molecular mass of the prodrug and the chemical identity was further confirmed by ^{1}H NMR.

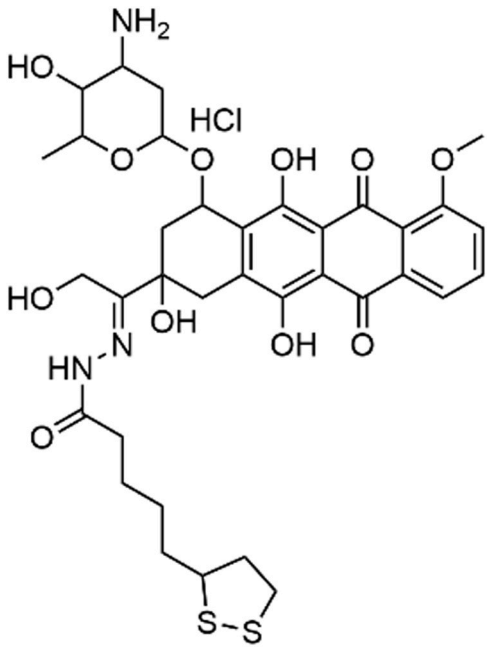

Scheme 1. Chemical structure of prodrug lipoyl-hydrazone-doxorubicin.

GNP production and characterization. TEM imaging showed that the GNPs prepared using a modified Turkevich method [27,28] had a size of ~16–17 nm and a near-spherical shape (Figure S1). FDGNPs were obtained by coating the GNPs with the functional components FA-PEG$_{3.5\,kDa}$-SH, BDP-PEG$_{2\,kDa}$-SH, lipoyl-hydrazone-Doxo and mPEG$_{2\,kDa}$-SH, which were used for targeting, tracking, intracellular pH-controlled drug release, and colloidal stability, respectively using a 50:20:1000:1000:1 FA-PEG$_{3.5\,kDa}$-SH/ BDP-PEG$_{2\,kDa}$-SH/ lipoyl-hydrazone-Doxo/ mPEG$_{2\,kDa}$-SH /GNPs molar ratios. The ratio of components was selected to achieve colloidal stability, high loading and targeting efficiency [25]. The conjugation yield of the components was derived indirectly upon isolation of the particles and assessment of the non-conjugated fractions in the supernatant according to studies reporting multifunctional GNP decoration [25,30]. Under the decoration condition set up, 100 % FA-PEG$_{3.5\,kDa}$-SH and BDP-PEG$_{2\,kDa}$-SH conjugation, 91 % of lipoyl-hydrazone-Doxo coupling and 87 % mPEG$_{2\,kDa}$-SH conjugation were obtained. Non-targeted and targeted Doxo-free nanoparticles were obtained by omitting FA-PEG$_{3.5\,kDa}$-SH during formulation, yielding DGNPs, or the lipoyl-hydrazone-Doxo, yielding FGNPs, respectively. Formulations were lyophilised with combination of cryoprotectants resulting in easy to redisperse dry products [24]. The UV/visible spectra of the reconstituted FDGNPs, DGNPs and FGNPs from the lyophilized versions showed an UV-Vis absorbance maximum at 520 nm, which is consistent with a particle core size of ~20 nm. There was also slight broadening of the spectra compared to the citrate-capped GNPs, which confirms the multifunctional coating and the colloidal integrity of the formulations [24]. DLS analyses revealed hydrodynamic particle sizes of about 35 nm for FDGNPs, DGNPs, and FGNPs, confirming the decoration of the particle core and indicating that PEG, the macromolecule common to the three formulations, is the main component responsible for the increase of hydrodynamic size compared to the naked GNPs (Fig. 1A). Transmission electron microscopy (TEM) confirmed the particle size and revealed a light grey corona on the dark metallic core of GNPs typical of PEG-coated metallic particles [30] (Fig. 1B).

The particle size and PDI remained unchanged over 48 h incubation in complete cell culture media, confirming their stability under physiological conditions (Fig. 1A). The pH-controlled release of Doxo from lipoyl-hydrazone-Doxo was assessed at pH 5.0 and 7.4 to mimic endosomal compartments, and blood and extracellular environments, respectively. At pH 5.0, Doxo was completely released within 48 h, whereas at pH 7.4, only ~13 % of drug was released (Fig. 1C). This result corroborates the microenvironmental pH-controlled drug release,

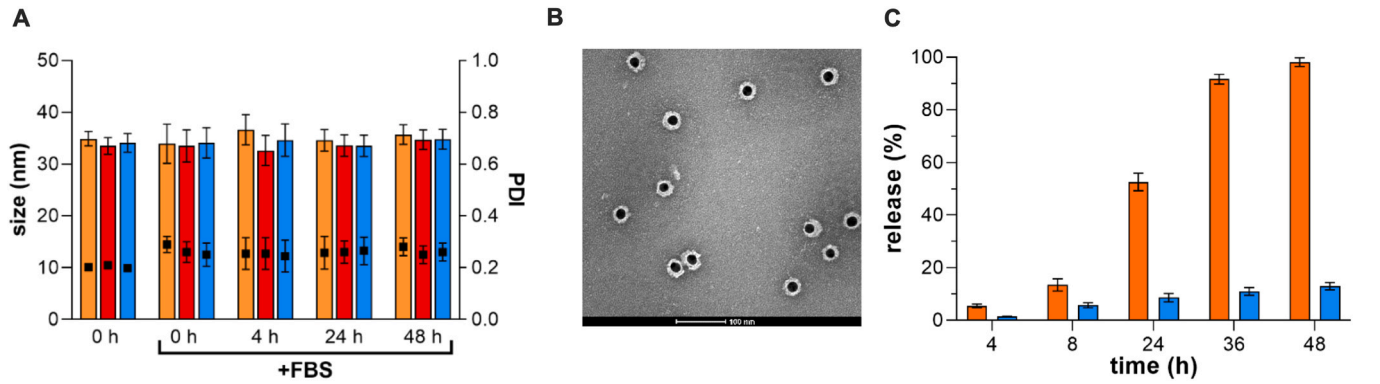

Fig. 1. Characterisation of the different GNP formulations. Size of FDGNP (orange bars), DGNP (red bars) and FGNP (blue bars) after reconstitution of the lyophilized versions in mQ water and upon incubation in folate free DMEM supplemented of 10 % FBS over time; PDI (■) refers to the right axis (A). Representative TEM images of FDGNPs; scale bar 100 nm (B). pH-dependent release of Doxo from lipoyl-hydrazone-Doxo in aqueous solution; Samples were incubated at pH 5 (orange bars) or 7.4 (blue bars) at 37 °C (C).

and the low drug release in blood prevents off-target toxic effects.

3.2. *Effect of free doxorubicin and folic acid-targeted doxorubicin-loaded gold nanoparticles on cell proliferation*

Before assessing the effect of FDGNPs on cancer cell proliferation, different cell lines commonly used to evaluate folate receptor (FR) targeting [31] were characterised for FR expression using a flow cytometric assay. As expected, the human breast cancer cell line, MCF7, did not express FR [32], whereas the human epidermoid carcinoma cell line KB expressed a low level of FR. However, KB cells cultured in a folic acid-free medium expressed significantly higher level of FR than MCF7 ($p \leq 0.0001$) and KB cells ($p \leq 0.01$). These cells were therefore named KB-hFR (Fig. 2A).

To verify the targeting capacity of FDGNPs compared to Doxo-loaded GNPs (DGNPs), the uptake of both was investigated in MCF7 and KB-hFR cells using a flow cytometric assay that exploited the Doxo fluorescence properties. In MCF7 cells, uptake of Doxo delivered as DGNPs or FR-targeted GNPs (FDGNPs) was very low at a Doxo concentration of 2 μM, with no statistically significant difference observed between untargeted and targeted GNPs at different incubation times (Fig. 2B). Interestingly, the highest level of Doxo uptake was observed in KB-hFR cells after 24 h of incubation with FR-targeted GNPs (FDGNPs) compared to the untargeted GNPs (DGNPs, $p \leq 0.001$) at the same Doxo concentration (2 μM), confirming the efficacy of the cell targeting of the proposed nanosystem (Fig. 2C). Based on PEG chain density on FDGNPs surface, PEG chains "brush-like" conformation is expected [33], which may prevent the folate from collapsing on the particle surface. These cellular studies therefore confirmed that coating nanoparticles with multiple components preserves the exposure of targeting ligands for cell biorecognition throughout the 24 h experimental setup, resulting in folate-dependent association with KB-hFR cells. Consequently, after 6 and 24 h of incubation, targeted nanoparticles associate with KB-hFR cells approximately four times more than non-targeted nanoparticles (Fig. 2C).

The effect of Doxo-loaded FR targeted GNPs (FDGNPs) on KB-hFR cell proliferation was compared to the effect of free Doxo. As shown in Fig. 3, free Doxo drug was able to induce a high level of toxicity in a dose- and time-dependent manner. Free Doxo exhibited a level of cytotoxicity greater than 20 % compared to untreated cells at a concentration of 1.0 μM after 24 h of incubation (32.55 % ± 6.23), reaching the highest level of cytotoxicity at the highest tested concentration of 10 μM after 72 h of incubation (45.58 % ± 9.43). In contrast, Doxo delivered as FDGNPs exhibited lower cytotoxicity, exceeding 20 % only at the highest tested concentration of 10 μM after 72 h of incubation (32.13 % ± 4.21). These data confirm the nanosystem's ability to control drug release. In line with the aforementioned release study, the system exhibits defined release kinetics, as opposed to the immediate availability observed with free Doxo [25,30]. This finding is particularly significant, as it demonstrates that the nanosystem can prevent uncontrolled Doxo release, thereby protecting healthy cells from off-target cytotoxicity and reducing related adverse effects.

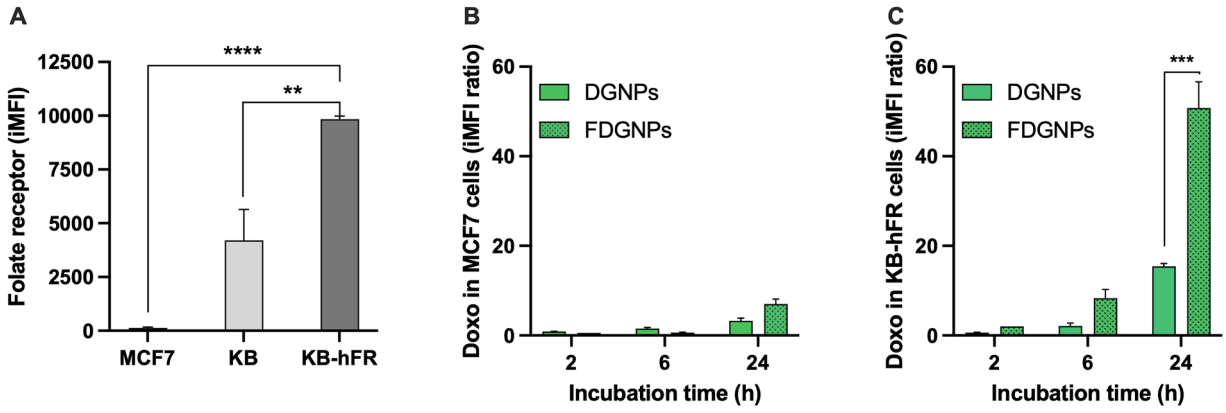

Fig. 2. Evaluation of folate receptor expression and Doxo uptake in various cell lines. Folate receptor (FR) expression was evaluated by flow cytometry in MCF7, KB and KB-hFR cells (A), and the cellular uptake of Doxo delivered as Doxo-loaded GNPs (DGNPs) or FR-targeted GNPs (FDGNPs) was evaluated using flow cytometry at different time points (2, 6 and 24 h) in MCF7 (B) and KB-hFR (C) cells. Data are shown as mean ± standard deviation (n = 3). Statistical significance between different conditions: ** $p \leq 0.01$, *** $p \leq 0.001$ and **** $p \leq 0.0001$.

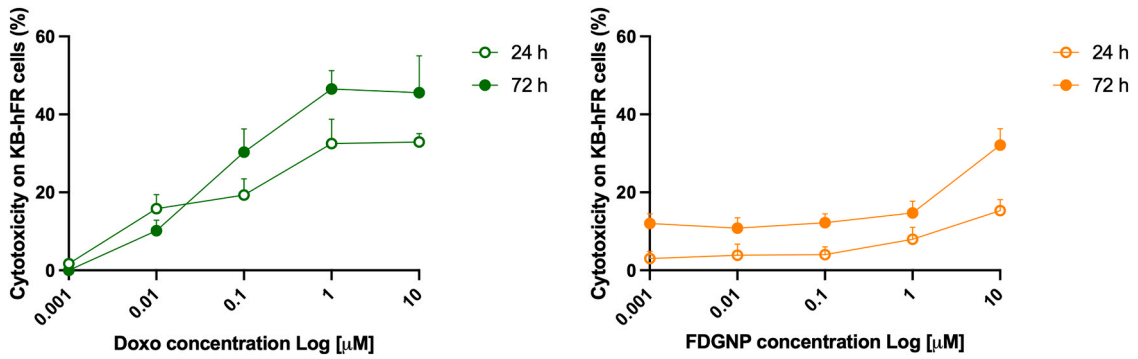

Fig. 3. Doxorubicin cytotoxicity as a free drug and as folate receptor-targeted Doxo-loaded GNPs in KB-hFR cells. KB-hFR cells were incubated at different Doxo concentrations (0.001, 0.01, 0.1, 1 and 10 μM) both as free drug or FDGNPs, and the WST-1 cell proliferation assay was used to investigate cytotoxicity at 24 and 72 h. Data are shown as mean ± standard deviation (n = 3).

To verify the delivery of Doxo by FDGNPs, fluorescence imaging was performed and compared with cells that had been incubated with free Doxo. Analysis of the imaging data showed that, after 24 h of incubation, Doxo added to cells as a free drug was mainly localised at the nuclear level (Fig. 4A-C), which explains the higher observed cytotoxicity (Fig. 3). Conversely, after 24 h of incubation, Doxo added to cells conjugated to FDGNPs was predominantly found in the cytoplasm in the form of green diffuse fluorescence (Fig. 4E-F). This is due to the slow sustained drug release by the endocytosed nanocarrier and may explain the lower observed cytotoxicity with respect to free Doxo (Fig. 3). Notably, only Doxo released from the particles can be revealed by confocal analysis, while Doxo conjugated to GNP undergoes florescence quenching, which prevents its detection [34].

3.3. Effect of US treatment on KB-hFR cells pre-incubated with folate receptor-targeted doxorubicin-loaded gold nanoparticles

The effect of the combined treatment using FDGNPs and US on KB-hFR cell proliferation was investigated by exposing FDGNPs, at an equivalent Doxo concentration of 2 μM, pre-incubated cells for 24 h to a specific US field. Significant decreases in cell proliferation were only observed following combined treatment with FGNPs or FDGNPs and US (Fig. 5A). Specifically, combined treatment with drug-free FGNPs and US resulted in a significant decrease in cell proliferation after 72 h, compared to untreated cells, cells treated with FGNPs only, and cells treated with US only ($p \leq 0.05$, Fig. 5A). Furthermore, the combined treatment with Doxo-loaded GNPs (FDGNPs, at an equivalent Doxo concentration of 2 μM) and US resulted in a significant decrease in cell proliferation after both 48 and 72 h, compared to untreated cells, cells treated with FDGNPs only, and cells treated with US only ($p \leq 0.01$ and $p \leq 0.001$, respectively; Fig. 5A). Interestingly, the combined treatment with FDGNPs and US resulted in a significantly greater decrease in cell proliferation than the combined treatment with drug-free GNPs (FGNPs) and US ($p \leq 0.01$, Fig. 5A). This suggests that, in the combined treatment with FDGNPs and US, the effect on cell proliferation can be attributed not only to US-activated GNPs, but also to the action of released Doxo, or possibly to US-activated Doxo.

As our previous works have shown that Doxo [21] and GNPs [19] can both be activated by US-mediated energy release to generate ROS, the ROS production induced by the combined treatment with FDGNPs and US was investigated. Fig. 5B shows a significant increase in ROS production starting at 1 min after treatment with FGNPs or FDGNPs and US,

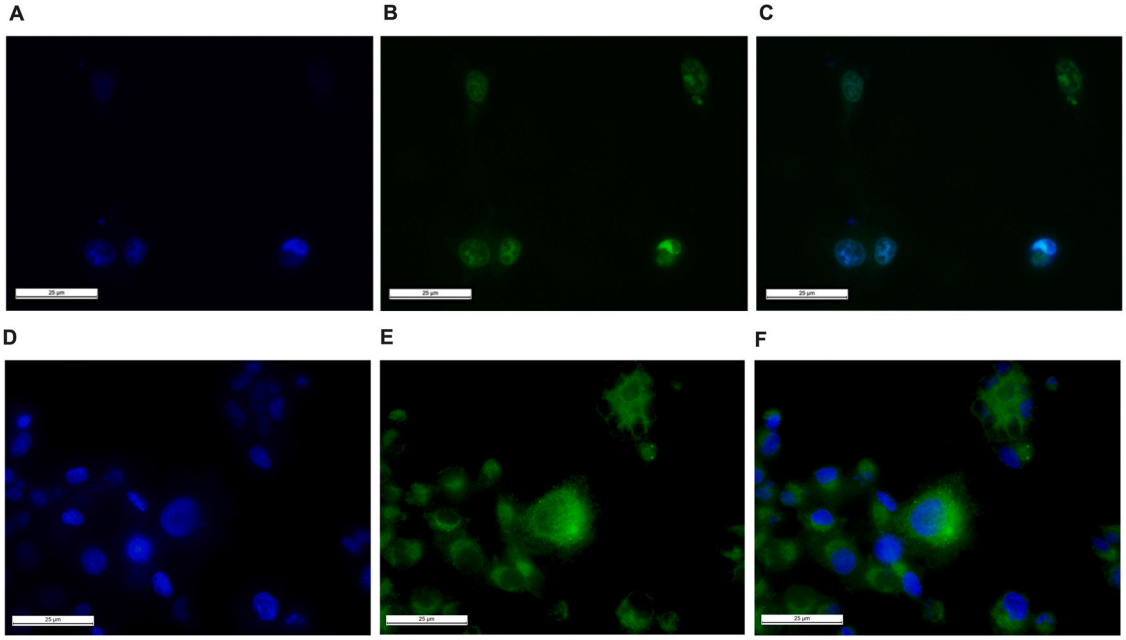

Fig. 4. Representative fluorescence microscopy images of doxorubicin disposition in KB-hFR cells exposed to the free drug or FDGNPs. KB-hFR cells were incubated with 2 μM Doxo (A-C) or FDGNPs at an equivalent concentration of Doxo for 24 h (D-F). The fluorescence images show the cell nuclei stained with DAPI (blue, A and D), intracellular Doxo (green, B and E) and an overlay of cell nuclei and intracellular Doxo (C and F). Magnification 63x; scale bars 25 μm.

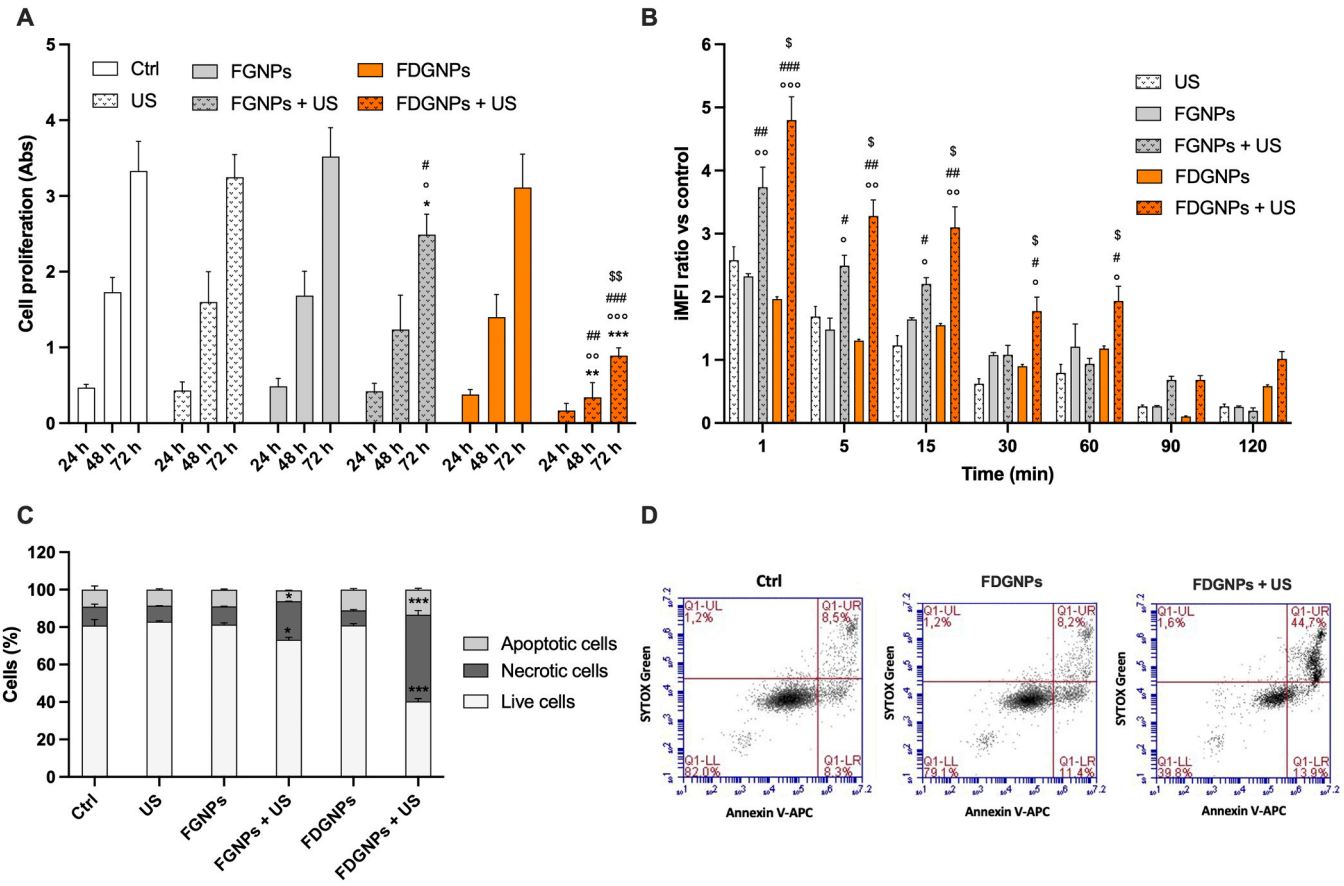

Fig. 5. Effect of US treatment on FDGNP pre-incubated KB-hFR cells. The cells were pre-incubated with FGNPs and FDGNPs at an equivalent Doxo concentration of 2 μM for 24 h, and then exposed to US (1.5 MHz, 0.11 W/cm^2, 50 % for 3 min). Cell proliferation after the different treatments (i.e., cells exposed to US only, cells exposed to FGNPs or FDGNPs only, and cells pre-incubated with FGNPs or FDGNPs and then exposed to US) was investigated at 24, 48 and 72 h using a WST-1 assay (A). ROS production after the different treatments was evaluated by flow cytometry using the CellROX® assay up to 120 min after treatments, as integrated mean fluorescence intensity (iMFI) ratio (B). Cell death after the different treatments was then investigated in KB-hFR cells 48 h after the treatment using the APC-Annexin V and Sytox® Green assay for flow cytometry (C) and representative dot plots (D) are shown. Data are shown as mean ± standard deviation (n = 3). Statistical significance versus untreated cells (Ctrl) *$p \leq 0.05$, **$p \leq 0.01$, ***$p \leq 0.001$; cells treated with US only °$p \leq 0.05$, °°$p \leq 0.01$, °°°$p \leq 0.001$; cells treated with FGNPs or FDGNPs only $^{\#}p \leq 0.05$, $^{\#\#}p \leq 0.01$, $^{\#\#\#}p \leq 0.001$ and cells treated with FGNPs and US $^{\$}p \leq 0.05$, $^{\$\$}p \leq 0.01$.

compared to treatment with US only ($p \leq 0.01$ and $p \leq 0.001$, respectively) and FGNPs or FDGNPs only ($p \leq 0.01$ and $p \leq 0.001$, respectively). A subsequent decrease in ROS production was then observed over time; however, the ROS levels remained significantly higher than those observed with US or nanosystems alone until 60 min after for the combined treatment with FDNPs and US, and until 15 min after the combined treatment with FGNPs and US (Fig. 5B). Interestingly, the combined treatment with FDGNPs and US resulted insignificantly higher ROS production levels than the combined treatment with drug-free GNPs (FGNPs) and US ($p \leq 0.05$, Fig. 5B). This suggests that the ROS production in the combined treatment with FDGNPs and US can be attributed not only to US-activated GNPs, but also to US-activated Doxo.

A flow cytometric assay was used to analyse the cell death induced by the combined treatment with FDGNPs and US. A significant decrease in the percentage of live cells, as well as a significant increase in the percentage of necrotic cells compared to untreated cells was observed 48 h after treatment compared to untreated cells (40.32 ± 1.51 and 80.86 ± 3.27, and 46.23 ± 2.22 and 10.12 ± 1.28, respectively; Fig. 5C-D). Notably, the combined treatment with drug-free FGNPs and US resulted in a lower decrease in the percentage of live cells and a lower increase in the percentage of necrotic cells than the combined treatment with FDGNPs and US (73.23 ± 1.32 and 40.32 ± 1.51, and 20.57 ± 0.90 and 46.23 ± 2.22, respectively; Fig. 5C-D).

Based on the significant necrotic cell death induced by US exposure in KB-hFR cells pre-incubated with FDGNPs, confocal microscopy imaging was performed to verify the intracellular disposition of Doxo after the US exposure. As expected, the intracellular localisation of the GNPs in KB-hFR cells, labelled with a specific fluorescent probe distinguishable from the fluorescent signal of the drug, was at the cytoplasmic level. This confirmed that the FDGNPs were taken up by the cells and appeared as red fluorescent dots mainly at the perinuclear level in the cytoplasm, while Doxo spread throughout the cytosol after 24 h of incubation, confirming its release (Fig. 6A-D). However, after US exposure of KB-hFR cells pre-incubated with FDGNPs for 24 h, the GNPs were still localised at the cytoplasmic level, whereas Doxo was not only spread in the cytosol, but also at the nuclear level compared to the pre-US irradiation (Fig. 6E-H). These data suggest that Doxo release from the FDGNPs may have been enhanced by US exposure, allowing it to diffuse to the cell nuclei.

3.4. Ultrasound field characterisation

A different device, the Esaote MyLab OMEGA US scanner, was selected to treat 3D cell cultures, specifically spheroids in their cell culture plates, without manipulation and with the ultimate goal to facilitate subsequent in vivo model experiments. To this end, the ultrasonic fields produced by the two devices were characterised to determine the optimal parameters for achieving the desired biological effects in the presence of significant differences in cell architecture. Table 1 summarises the US field parameters used for the 2D and 3D cell culture

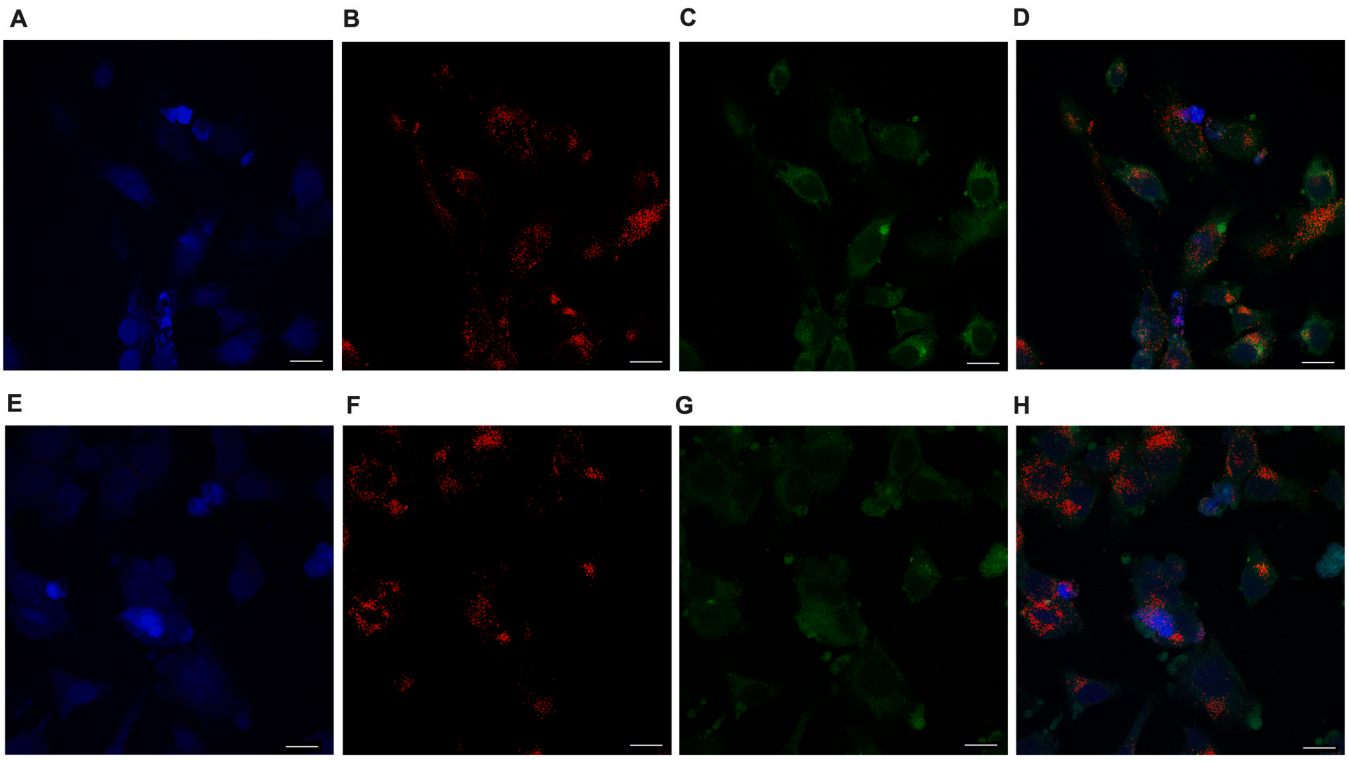

Fig. 6. Representative confocal images of doxorubicin and GNPs in KB-hFR cells pre-incubated with FDGNPs (at an equivalent Doxo concentration of 2 μM) and then exposed to US. Images of KB-hFR cells incubated with FDGNPs for 24 h (A-D). The images show the cell nuclei stained with DAPI (blue, A), FR-targeted GNPs labelled with BODIPY (red, B), Doxo (green, C), and an overlay of cell nuclei, FR-targeted GNPs and Doxo (D). Magnification 40x and; scale bars 25 μm. Images of KB-hFR cells pre-incubated with FDGNPs for 24 h, then exposed to US (1.5 MHz, 0.11 W/cm^2, 50 % for 3 min) (E-H), showing cell nuclei stained with DAPI (blue, E), FR-targeted GNPs labelled with BODIPY (red, F), Doxo (green, G), and an overlay of cell nuclei, FR-targeted GNPs and Doxo (H). Magnification 40x; scale bars 25 μm.

experiments.

3.5. Effect of US treatment on the viability of KB-hFR spheroids pre-incubated with folate receptor-targeted doxorubicin-loaded gold nanoparticles

KB-hFR spheroids were pre-incubated for 24 h with FGNPs and FDGNPs at an equivalent Doxo concentration of 4 μM. The spheroids were then exposed to an US field generated by a standardised US scanner (Fig. 7B-C). A higher concentration of Doxo and of the equivalent concentration of FR-targeted drug-free GNPs was used compared to the treatment of 2D KB-hFR cell cultures, due to the higher cell density of the 3D cell spheroids. The combined FDGNPs and US treatment resulted in a significant decrease in spheroid viability, as determined by ATP-based metabolic activity, compared to untreated spheroids and spheroids treated with US, FGNPs or FDGNPs only ($p \leq 0.01$), and the combined treatment with FGNPs and US, 48 h after the treatment ($p \leq 0.05$; Fig. 7C). Moreover, the combined treatment with drug-free FGNPs and US significantly decreased the cell viability of KB-hFR spheroids compared to the other treatments, albeit to a lesser extent than the combined treatment with FDGNPs and US (Fig. 7C).

Notably, the US setup based on a standardised US scanner (Fig. 7B-C) was able to generate the required amount of energy in 3D cultures to replicate the results obtained with a custom-built device in 2D cell cultures (Fig. 5A).

Table 1
US field parameters.

Device	Peak Positive Pressure (MPa)	ISPTA (W/cm^2)	Mechanical Index
2D cell cultures	0.26	0.11	0.22
3D cell cultures	1.33	0.26	0.44

4. Discussion

FDGNPs have been designed to enhance the site-specific anticancer activity of doxorubicin through a combined approach. This involves targeting FR-positive cancer cells using folic acid conjugation, as well as achieving controlled doxorubicin release and ROS production at the tumour site upon US exposure by combining pH-sensitive and US-triggerable moieties. FDGNPs display high selectivity for FR-overexpressing cells and exhibit time-dependent cell uptake (Fig. 2). This could lead to improved clinical outcomes with reduced off-target side effects. Conjugation of Doxo to GNPs via a pH-sensitive linker enables drug release under acidic endosomal conditions, thereby preventing systemic toxicity. In contrast, the unformulated drug is indiscriminately taken up by cells and localises in the cell nucleus (Figs. 3 and 4). It is worth mentioning that GNPs can be cleared from the body via the hepatobiliary system, thereby preventing accumulation-associated toxicity [35–37].

Activation of the system using US was found to significantly enhance its cytotoxicity, reducing cancer cell viability by approximately 70 % 72 h after treatment (Fig. 5A). As previously reported [19], ROS production due to GNP US triggering exploits the unique property of GNPs to absorb US energy, resulting in local heating [38] and/or inducing ROS production in the so-called sonodynamic effect [19,39]. This effectively results in cell destruction in the targeted areas, with the induced cytotoxicity primarily correlating to an increase in necrotic cancer cell death (Fig. 5C-D). Notably, when the data are analysed collectively, it should be noted that the decrease in cancer cell

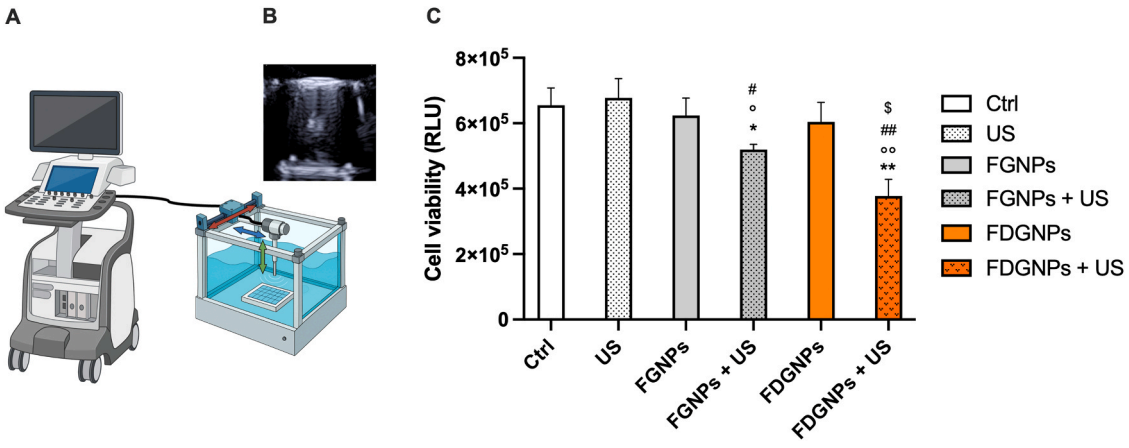

Fig. 7. Effect of US treatment on the viability of FDGNP pre-incubated KB-hFR spheroids. The spheroids were pre-incubated with FDGNPs equivalent to a 4 μM concentration of Doxo for 24 h, and then exposed to US (1.7 MHz, 0.26 W/cm^2, 50 %, for 5 min). A simplified scheme of the US setup (A) and a representative US scanning image of a well containing a KB-hFR spheroid during US exposure (B). Cell viability was investigated 48 h after the treatment using an ATP assay (C). Data are shown as mean ± standard deviation (n = 3). Statistical significance versus untreated cells (Ctrl) *p ≤ 0.05, **p ≤ 0.01; cells treated with US only °p ≤ 0.05, °°p ≤ 0.01; cells treated with FGNPs or FDGNPs only $^{\#}$p ≤ 0.05, $^{\#\#}$p ≤ 0.01, and cells treated with FGNPs and US $^{\$}$p ≤ 0.05.

proliferation was attributed to US-induced ROS production by both GNPs and Doxo, which confirms previous results that highlight the US responsiveness of doxorubicin [21]. Additionally, the intracellular localisation of the different US-responsive agents, i.e. GNPs and Doxo, revealed that, surprisingly, enhanced Doxo release from the GNPs cannot be excluded after US exposure, as demonstrated by imaging analysis showing increased drug accumulation in the cell nuclei compared to the cells not exposed to US (Fig. 6).

Recently, Hornsby et al. developed a kinetic model to study the release of doxorubicin adsorbed onto GNPs through non-covalent electrostatic and hydrophobic interactions upon US exposure. This model highlights the significant effect of US on drug dissociation from the GNP surface, primarily driven by acoustic radiation force [40]. Moreover, a multiphysics model was developed and validated using an ex vivo model to predict the threshold for doxorubicin release from GNPs when exposed to US [41]. However, the doxorubicin-loaded GNPs used by Hornsby et al. [40,41], exhibited limited cancer selectivity and quite rapid uncontrolled drug release, even in the absence of external stimuli, in contrast to the system reported in the present work.

The novelty of FDGNPs described in the present study lies in the integration of targeting agents with a pH- and US-controlled release mechanism of anticancer drugs chemically conjugated to GNPs and ROS production, whose interplay results in a uniquely enhanced therapeutic effect while ensuring low off-target drug release. Consequently, the risk of cytotoxic drug leakage from the nanocarrier and the damage to healthy tissues are minimised by the controlled-release mechanism of the FDGNPs, which is inactive at physiological pH. In the literature, another interesting US triggerable drug-free GNP hybrid system has been reported. In this formulation, GNPs were combined with perfluorohexane and cetuximab, a chimeric monoclonal antibody that selectively inhibits the epidermal growth factor receptor (EGFR), as targeting moiety [42]. It is worth noting that the FDGNP formulation described in the present work uses folic acid conjugation to overcome the potential drawbacks associated with monoclonal antibodies, such as their high cost and possible immunogenicity, while also incorporating a chemically conjugated anticancer drug designed for acid pH- and US triggered release.

Moreover, it cannot be ruled out that the increased US-mediated cytotoxicity observed following exposure to US after FDGNP treatment is due to the combined effect of the significant increase in ROS caused by GNPs and Doxo activation by US exposure (Fig. 5), as well as enhanced intracellular Doxo release (Fig. 6). This means that the localised US-induced ROS generation could have an additive effect to the cytotoxic activity of the chemotherapeutic drug, making it a powerful combination for treating solid tumours. The observed US-mediated cytotoxicity of FDGNPs, together with the greater increase in US-mediated ROS generation, confirms the ability of FDGNPs to act as a nano-sonosensitiser, eliciting sonodynamic activity [19,43]. In a previous work [19], we observed that folate-PEG-decorated GNPs could induce significant ROS production under US exposure, in the same in vitro cell model. In that study, ROS production depended on the US energy used and the density of particles present in the cells. Furthermore, a different probe was used to quantify ROS generation compared to in this study, thereby reinforcing the US-mediated ROS generation highlighted herein.

These results were confirmed by using a standardised US scanner on KB-hFR spheroids to obtain an US field capable of translating in 3D cell cultures the biological effects obtained in 2D cell cultures (Fig. 7). Indeed, the treatment with the standardised US scanner significantly reduced the viability of FDGNP-treated spheroids by around 45 %. It is worth emphasising that the standardised US scanner can localise the target through imaging and trigger a sonodynamic effect in a more complex in vitro cancer model that more closely mimics cancer tissue (i.e., spheroids). These findings validate the design of our nanoplatform and provide robust proof-of-concept that properly standardised US systems have the potential to activate responsive agents (i.e., sono-sensitisers) in more realistic in vivo tumour models. This can be achieved by selecting specific US modalities that are already available and adopted for diagnostic purpose (i.e., US imaging). This overcomes a long-standing limitation in the field: variability in acoustic exposure and lack of comparability between studies.

Finally, while this study primarily focused on the therapeutic effects, the theranostic potential of GNPs is also noteworthy. Their strong optical and acoustic properties make them suitable for real-time imaging techniques, such as photoacoustic imaging or surface-enhanced Raman spectroscopy (SERS), which enable simultaneous treatment monitoring [44,45]. Future work should explore how commercial US platforms may facilitate such theranostic applications.

5. Conclusion

Gold nanoparticles can be engineered to exploit active targeting, stimuli-responsive drug delivery, and sonosensitising properties enabling precise, US-guided cancer treatment. Our results demonstrate that FDGNPs: i) selectively target FR-overexpressing cancer cells, ii) efficiently deliver doxorubicin with spatial control in both 2D and 3D

cancer cell models, depending on the pH environment and US exposure, and iii) significantly increase the cytotoxicity of doxorubicin through the generation of ROS by US exposure. Moreover, we show that a standardised US scanner can be used to effectively activate a sonodynamic nanoplatform in 3D cancer spheroids.

This significant advancement bridges the gap between preclinical research and in vivo applicability, offering a translatable, reproducible, and scalable approach to US-based cancer therapy. Indeed, by integrating a standardised US device into the experimental pipeline, our work sets the foundation for future in vivo studies, bringing us closer to a new generation of US-guided, non-invasive, and highly selective cancer treatments.

CRediT authorship contribution statement

Federica Foglietta: Writing – original draft, Investigation, Formal analysis, Data curation. **Agnese Fragassi:** Investigation, Formal analysis. **Cristiano Pesce:** Investigation, Formal analysis. **Francisco Andres Soto Arratia:** Investigation, Formal analysis. **Alberto Mangia:** Methodology. **Maurizio Giustetto:** Methodology. **Gianni Durando:** Resources, Methodology, Formal analysis. **Gian Matteo Morano:** Methodology, Formal analysis. **Paolo Caliceti:** Validation, Supervision. **Andrea Grandoni:** Validation, Resources, Methodology. **Roberto Canaparo:** Writing – original draft, Validation, Funding acquisition, Conceptualization. **Loredana Serpe:** Writing – review & editing, Supervision, Conceptualization. **Stefano Salmaso:** Writing – review & editing, Supervision, Conceptualization.

Funding

This work was supported by the Univeristy of Torino, Italy (grant Ricerca Locale 2023 and Ricerca Locale 2024) and by NextGeneration EU DD. 3175/2021 E DD. 3138/2021 CN3 through the “National Center for Gene Therapy and Drugs based on RNA Technology” (Project no. CN00000041 CN3, Spoke #8 “Platforms for RNA/DNA delivery”).

Declaration of Competing Interest

The authors declare that they have no known competing financial interests or personal relationships that could have appeared to influence the work reported in this paper.

Appendix A. Supporting information

Supplementary data associated with this article can be found in the online version at doi:10.1016/j.biopha.2025.118777.

Data Availability

Data will be made available on request.

References

[1] C. Carvalho, R. Santos, S. Cardoso, S. Correia, P. Oliveira, M. Santos, P. Moreira, Doxorubicin: the good, the bad and the ugly effect, Curr. Med Chem. 16 (2009) 3267–3285, https://doi.org/10.2174/092986709788803312.
[2] H. Sabit, M. Abdel-Hakeem, T. Shoala, S. Abdel-Ghany, M.M. Abdel-Latif, J. Almulhim, M. Mansy, Nanocarriers: a reliable tool for the delivery of anticancer drugs, Pharmaceutics 14 (2022) 1566, https://doi.org/10.3390/pharmaceutics14081566.
[3] J.K. Patra, G. Das, L.F. Fraceto, E.V.R. Campos, M. del P. Rodriguez-Torres, L. S. Acosta-Torres, L.A. Diaz-Torres, R. Grillo, M.K. Swamy, S. Sharma, S. Habtemariam, H.-S. Shin, Nano based drug delivery systems: recent developments and future prospects, J. Nanobiotechnology 16 (2018) 71, https://doi.org/10.1186/s12951-018-0392-8.
[4] A.S. Hoffman, The origins and evolution of “controlled” drug delivery systems, J. Control. Release 132 (2008) 153–163, https://doi.org/10.1016/j.jconrel.2008.08.012.
[5] P. Ebrahimnejad, A. Sodagar Taleghani, K. Asare-Addo, A. Nokhodchi, An updated review of folate-functionalized nanocarriers: A promising ligand in cancer, Drug Discov. Today 27 (2022) 471–489, https://doi.org/10.1016/j.drudis.2021.11.011.
[6] B. Farran, R.C. Montenegro, P. Kasa, E. Pavitra, Y.S. Huh, Y.-K. Han, M.A. Kamal, G.P. Nagaraju, G.S. Rama Raju, Folate-conjugated nanovehicles: Strategies for cancer therapy, Materials Science Engineering C 107 (2020) 110341, https://doi.org/10.1016/j.msec.2019.110341.
[7] E.T. Kim, J.H. Kim, E.Y. Park, I.H. Song, H.S. Park, S. Park, M.C. Lim, The Efficacy and Safety of Folate Receptor α-Targeted Antibody-Drug Conjugate Therapy in Patients With High-Grade Epithelial Ovarian, Primary Peritoneal, or Fallopian Tube Cancers: A Systematic Review and Meta-Analysis, Cancer Med 13 (2024), https://doi.org/10.1002/cam4.70392.
[8] B. Bahrami, M. Mohammadnia-Afrouzi, P. Bakhshaei, Y. Yazdani, G. Ghalamfarsa, M. Yousefi, S. Sadreddini, F. Jadidi-Niaragh, M. Hojjat-Farsangi, Folate-conjugated nanoparticles as a potent therapeutic approach in targeted cancer therapy, Tumor Biol. 36 (2015) 5727–5742, https://doi.org/10.1007/s13277-015-3706-6.
[9] P. Davoodi, L.Y. Lee, Q. Xu, V. Sunil, Y. Sun, S. Soh, C.-H. Wang, Drug delivery systems for programmed and on-demand release, Adv. Drug Deliv. Rev. 132 (2018) 104–138, https://doi.org/10.1016/j.addr.2018.07.002.
[10] J.A. Moore, J.C.L. Chow, Recent progress and applications of gold nanotechnology in medical biophysics using artificial intelligence and mathematical modeling, Nano Express 2 (2021) 022001, https://doi.org/10.1088/2632-959X/abddd3.
[11] Y. Du, L. Xia, A. Jo, R.M. Davis, P. Bissel, M.F. Ehrich, D.G.I. Kingston, Synthesis and Evaluation of Doxorubicin-Loaded Gold Nanoparticles for Tumor-Targeted Drug Delivery, Bioconjug Chem. 29 (2018) 420–430, https://doi.org/10.1021/acs.bioconjchem.7b00756.
[12] A.H. Faid, S.A. Shouman, Y.A. Badr, M. Sharaky, Enhanced cytotoxic effect of doxorubicin conjugated gold nanoparticles on breast cancer model, BMC Chem. 16 (2022) 90, https://doi.org/10.1186/s13065-022-00889-9.
[13] T. Cui, J.-J. Liang, H. Chen, D.-D. Geng, L. Jiao, J.-Y. Yang, H. Qian, C. Zhang, Y. Ding, Performance of doxorubicin-conjugated gold nanoparticles: regulation of drug location, ACS Appl. Mater. Interfaces 9 (2017) 8569–8580, https://doi.org/10.1021/acsami.6b16669.
[14] F. Wang, Y.-C. Wang, S. Dou, M.-H. Xiong, T.-M. Sun, J. Wang, Doxorubicin-tethered responsive gold nanoparticles facilitate intracellular drug delivery for overcoming multidrug resistance in cancer cells, ACS Nano 5 (2011) 3679–3692, https://doi.org/10.1021/nn200007z.
[15] S. Aryal, J.J. Grailer, S. Pilla, D.A. Steeber, S. Gong, Doxorubicin conjugated gold nanoparticles as water-soluble and pH-responsive anticancer drug nanocarriers, J. Mater. Chem. 19 (2009) 7879, https://doi.org/10.1039/b914071a.
[16] D. Liu, F. Yang, F. Xiong, N. Gu, The smart drug delivery system and its clinical potential, Theranostics 6 (2016) 1306–1323, https://doi.org/10.7150/thno.14858.
[17] N.M. AlSawaftah, N.S. Awad, W.G. Pitt, G.A. Husseini, pH-responsive nanocarriers in cancer therapy, Polymers 14 (2022) 936, https://doi.org/10.3390/polym14050936.
[18] Y. Mu, L. Gong, T. Peng, J. Yao, Z. Lin, Advances in pH-responsive drug delivery systems, OpenNano 5 (2021) 100031, https://doi.org/10.1016/j.onano.2021.100031.
[19] C. Brazzale, R. Canaparo, L. Racca, F. Foglietta, G. Durando, R. Fantozzi, P. Caliceti, S. Salmaso, L. Serpe, Enhanced selective sonosensitizing efficacy of ultrasound-based anticancer treatment by targeted gold nanoparticles, Nanomedicine 12 (2016), https://doi.org/10.2217/nnm-2016-0293.
[20] F. Foglietta, M. Giacone, G. Durando, R. Canaparo, L. Serpe, Sonodynamic treatment triggers cancer cell killing by doxorubicin in p-glycoprotein-mediated multidrug resistant cancer models, Adv. Ther. (Weinh.) (2024), https://doi.org/10.1002/adtp.202400070.
[21] F. Foglietta, M. Macrì, P. Panzanelli, A. Francovich, G. Durando, F. Garello, E. Terreno, L. Serpe, R. Canaparo, Ultrasound boosts doxorubicin efficacy against sensitive and resistant ovarian cancer cells, Eur. J. Pharm. Biopharm. 183 (2023) 119–131, https://doi.org/10.1016/j.ejpb.2023.01.005.
[22] N. Choubdar, S. Avizheh, S.A. Karimifard, Recent Advances in Efficacy of using Doxorubicin Gold Nanoparticles for Chemo-, Radio-, Photothermal, and Photodynamic Therapy, Curr. Drug Deliv. 19 (2022) 745–762, https://doi.org/10.2174/1567201818666210707110742.
[23] A. Raza, U. Hayat, T. Rasheed, M. Bilal, H.M.N. Iqbal, “Smart” materials-based near-infrared light-responsive drug delivery systems for cancer treatment: A review, J. Mater. Res. Technol. 8 (2019) 1497–1509, https://doi.org/10.1016/j.jmrt.2018.03.007.
[24] I. Goemaere, A. Cielo, R. Daniele, F. Mastrotto, S.C. De Smedt, W.H. De Vos, S. Salmaso, K. Braeckmans, Nanosecond Laser Pulses Facilitating Efficient and Specific Cell Killing with Doxorubicin-Loaded Gold Nanoparticles Targeted to the Folate Receptor, Small Sci. 5 (2025), https://doi.org/10.1002/smsc.202400234.
[25] C. Brazzale, F. Mastrotto, P. Moody, P.D. Watson, A. Balasso, A. Malfanti, G. Mantovani, P. Caliceti, C. Alexander, A.T. Jones, S. Salmaso, Control of targeting ligand display by pH-responsive polymers on gold nanoparticles mediates selective entry into cancer cells, Nanoscale 9 (2017) 11137–11147, https://doi.org/10.1039/C7NR02595E.
[26] G.E.C. Sims, T.J. Snape, A method for the estimation of polyethylene glycol in plasma protein fractions, Anal. Biochem 107 (1980) 60–63, https://doi.org/10.1016/0003-2697(80)90492-3.
[27] S.P.C, H.J, J. Turkevich, The Formation of Colloidal Gold, J. Phys. Chem. (1953) 670.
[28] C. Li, D. Li, G. Wan, J. Xu, W. Hou, Facile synthesis of concentrated gold nanoparticles with low size-distribution in water: temperature and pH controls, Nanoscale Res Lett. 6 (2011) 440, https://doi.org/10.1186/1556-276X-6-440.

[29] X. Liu, M. Atwater, J. Wang, Q. Huo, Extinction coefficient of gold nanoparticles with different sizes and different capping ligands, Colloids Surf. B Biointerfaces 58 (2007) 3–7, https://doi.org/10.1016/j.colsurfb.2006.08.005.
[30] R. Daniele, C. Brazzale, B. Arpac, F. Tognetti, C. Pesce, A. Malfanti, E. Sayers, F. Mastrotto, A.T. Jones, S. Salmaso, P. Caliceti, Influence of Folate-Targeted Gold Nanoparticles on Subcellular Localization and Distribution into Lysosomes, Pharmaceutics 15 (2023) 864, https://doi.org/10.3390/pharmaceutics15030864.
[31] F. Sonvico, C. Dubernet, V. Marsaud, M. Appel, H. Chacun, B. Stella, M. Renoir, P. Colombo, P. Couvreur, Establishment of an in vitro model expressing the folate receptor for the investigation of targeted delivery systems, J. Drug Deliv. Sci. Technol. 15 (2005) 407–410, https://doi.org/10.1016/S1773-2247(05)50080-7.
[32] E. Gallon, T. Matini, L. Sasso, G. Mantovani, A. Armiñan de Benito, J. Sanchis, P. Caliceti, C. Alexander, M.J. Vicent, S. Salmaso, Triblock Copolymer Nanovesicles for pH-Responsive Targeted Delivery and Controlled Release of siRNA to Cancer Cells, Biomacromolecules 16 (2015) 1924–1937, https://doi.org/10.1021/acs.biomac.5b00286.
[33] Z. Ma, D.N. LeBard, S.M. Loverde, K.A. Sharp, M.L. Klein, D.E. Discher, T.H. Finkel, TCR Triggering by pMHC Ligands Tethered on Surfaces via Poly(Ethylene Glycol) Depends on Polymer Length, PLoS One 9 (2014) e112292, https://doi.org/10.1371/journal.pone.0112292.
[34] V. Ramalingam, K. Varunkumar, V. Ravikumar, R. Rajaram, Target delivery of doxorubicin tethered with PVP stabilized gold nanoparticles for effective treatment of lung cancer, Sci. Rep. 8 (2018) 3815, https://doi.org/10.1038/s41598-018-22172-5.
[35] E. Sadauskas, G. Danscher, M. Stoltenberg, U. Vogel, A. Larsen, H. Wallin, Protracted elimination of gold nanoparticles from mouse liver, Nanomedicine 5 (2009) 162–169, https://doi.org/10.1016/j.nano.2008.11.002.
[36] M. Longmire, P.L. Choyke, H. Kobayashi, Clearance properties of nano-sized particles and molecules as imaging agents: considerations and caveats, Nanomedicine 3 (2008) 703–717, https://doi.org/10.2217/17435889.3.5.703.
[37] J.H. Park, N. Oh, Endocytosis and exocytosis of nanoparticles in mammalian cells, Int J. Nanomed. (2014) 51, https://doi.org/10.2147/IJN.S26592.
[38] X. Pan, L. Bai, H. Wang, Q. Wu, H. Wang, S. Liu, B. Xu, X. Shi, H. Liu, Metal–Organic-framework-derived carbon nanostructure augmented sonodynamic cancer therapy, Adv. Mater. 30 (2018), https://doi.org/10.1002/adma.201800180.
[39] S. George, L. Serpe, Exploring the redox potential induced by low-intensity focused ultrasound on tumor masses, Life Sci. 332 (2023) 122040, https://doi.org/10.1016/j.lfs.2023.122040.
[40] T.K. Hornsby, F.M. Kashkooli, A. Jakhmola, M.C. Kolios, J. Tavakkoli, Kinetic modelling of ultrasound-triggered chemotherapeutic drug release from the surface of gold nanoparticles, Sci. Rep. 13 (2023) 21301, https://doi.org/10.1038/s41598-023-48082-9.
[41] T.K. Hornsby, F.M. Kashkooli, A. Jakhmola, M.C. Kolios, J. (Jahan) Tavakkoli, Multiphysics modeling of low-intensity pulsed ultrasound induced chemotherapeutic drug release from the surface of gold nanoparticles, Cancers (Basel) 15 (2023) 523, https://doi.org/10.3390/cancers15020523.
[42] Y. Ma, X. Peng, L. Wang, H. Li, W. Cheng, X. Zheng, Y. Liu, Cetuximab-conjugated perfluorohexane/gold nanoparticles for low intensity focused ultrasound diagnosis ablation of thyroid cancer treatment, Sci. Technol. Adv. Mater. 21 (2020) 856–866, https://doi.org/10.1080/14686996.2020.1855064.
[43] L. Huang, Y. Su, X. Hu, Y. Zhang, G. Xu, S. Chen, J. Wu, S. Wang, D. Zhang, Z. Zeng, S. Hong, X. Lin, An ultrasound-activated nanozyme sonosensitizer for photoacoustic imaging-guided breast cancer sonodynamic and starvation combination therapy, ACS Appl. Nano Mater. 7 (2024) 4441–4452, https://doi.org/10.1021/acsanm.3c05959.
[44] Y. Hang, A. Wang, N. Wu, Plasmonic silver and gold nanoparticles: shape- and structure-modulated plasmonic functionality for point-of-caring sensing, bio-imaging and medical therapy, Chem. Soc. Rev. 53 (2024) 2932–2971, https://doi.org/10.1039/D3CS00793F.
[45] R.S. Riley, E.S. Day, Gold nanoparticle-mediated photothermal therapy: applications and opportunities for multimodal cancer treatment, WIREs Nanomed. Nanobiotechnol. 9 (2017), https://doi.org/10.1002/wnan.1449.